

# Modeling High-Velocity QSO Absorbers with Photoionized MHD Disk-Winds

KEIGO FUKUMURA<sup>1,2,3</sup>, DEMOSTHENES KAZANAS<sup>3</sup>, IOANNIS CONTOPOULOS<sup>4</sup>,  
AND  
EHUD BEHAR<sup>5</sup>

## ABSTRACT

We extend our modeling of the ionization structure of magnetohydrodynamic (MHD) accretion-disk winds, previously applied to Seyfert galaxies, to a population of quasi-stellar-objects (QSOs) of much lower X-ray-to-UV flux ratios, i.e. smaller  $\alpha_{\text{ox}}$  index, motivated by UV/X-ray ionized absorbers with extremely high outflow velocities in UV-luminous QSOs. We demonstrate that magnetically-driven winds ionized by a spectrum with  $\alpha_{\text{ox}} \simeq -2$  can produce the charge states responsible for C IV and Fe XXV/Fe XXVI absorption in wind regions with corresponding maximum velocities of  $v(\text{C IV}) \lesssim 0.1c$  and  $v(\text{Fe xxv}) \lesssim 0.6c$  (where  $c$  is the speed of light) and column densities  $N_H \sim 10^{23} - 10^{24} \text{ cm}^{-2}$ , in general agreement with observations. In contrast to the conventional radiation-driven wind models, *high-velocity flows are always present in our MHD-driven winds* but manifest in the absorption spectra only for  $\alpha_{\text{ox}} \lesssim -2$ , as larger  $\alpha_{\text{ox}}$  values ionize the wind completely out to radii too large to demonstrate the presence of these high velocities. We thus predict increasing velocities of these ionized absorbers with decreasing (steeper)  $\alpha_{\text{ox}}$ , a quantity that emerges as the defining parameter in the kinematics of the AGN UV/X-ray absorbers.

*Subject headings:* accretion, accretion disks — galaxies: active — methods: numerical — quasars: absorption lines — X-rays: galaxies

---

<sup>1</sup>Email: Keigo.Fukumura@nasa.gov

<sup>2</sup>University of Maryland, Baltimore County (UMBC/CRESST), Baltimore, MD 21250

<sup>3</sup>Astrophysics Science Division, NASA/Goddard Space Flight Center, Greenbelt, MD 20771

<sup>4</sup>Research Center for Astronomy, Academy of Athens, Athens 11527, Greece

<sup>5</sup>Department of Physics, Technion, Haifa 32000, Israel

## 1. Introduction

The launch of *Chandra* and *XMM-Newton* ushered a new era in X-ray astronomy of AGN outflows with the discovery of absorption lines in the spectra that enabled for the first time accurate charge state and velocity measurements. The long observations of a number of AGNs revealed transitions of charge states as diverse as Fe I through Fe XXVI. Since any atomic gas with bound electrons absorbs X-rays these ions span a range of  $\sim 10^5$  in ionization parameter<sup>1</sup>  $\xi$ , a fact that underscores the great utility of X-ray spectroscopy.

In a subsequent development, Holczer, Behar & Kaspi (2007) and Behar (2009, hereafter, B09) developed a statistical measure of the plethora of the transitions in the *Chandra/XMM* spectra, the absorption measure distribution (AMD), namely the differential hydrogen-equivalent column  $N_H$  of specific ions per decade of  $\xi$ , i.e.  $\text{AMD} \equiv dN_H/d\log \xi$ . Moreover, the AMD was found to be roughly constant, i.e.  $N_H$  to be roughly independent of  $\xi$ , in the small number of Seyferts for which the data quality allowed a quantitative analysis. The functional form of the AMD is significant as it can provide the plasma density along the observer’s line of sight (LoS), which for constant AMD is  $n(r) \propto r^{-1}$ .

Motivated by the AMD systematics, Fukumura et al. (2010, hereafter, FKCB) employed the photoionization code *XSTAR* (Kallman & Bautista 2001) to determine the ionization structure of the 2D winds of Contopoulos & Lovelace (1994, hereafter, CL94) which provide for density profiles such as  $n \propto r^{-1}$ . This density dependence on  $r$  yields also  $\xi \propto r^{-1}$ , thereby allowing for ionic species of decreasing ionization with distance, but of columns similar to those of high ionization. Importantly, these models are scale free: with the radial coordinate  $r$  normalized to the Schwarzschild radius,  $r_s$ , and the mass flux to the Eddington rate,  $\xi$  is independent of the black hole mass  $M$ , implying broad applicability in galactic and extragalactic settings. Assuming an ionizing spectral energy density (SED) of  $F_\nu \propto \nu^{-1}$  between 1 and 1000 Ryd, these models were successful in reproducing the observed: (i) Slow velocities ( $v \sim 100 - 300 \text{ km s}^{-1}$ ) for the low ionization transitions like Fe XVII and fast outflows ( $v \sim 1,000 - 3,000 \text{ km s}^{-1}$ ) for the high ionization ones such as Fe XXV, and (ii) AMD almost independent of  $\xi$  for  $-1 \lesssim \log \xi \lesssim 4$ , in agreement with the results of B09.

While X-ray absorption lines in Seyfert spectra are rather recent discoveries, UV absorption lines in Seyferts and QSOs have been known (e.g., Crenshaw et al. 2003; Brandt, Laor, & Wills 2000). Also known since the earlier *ROSAT* surveys (e.g. Kopko et al. 1994; Green & Mathur 1996) is that the X-ray-to-UV flux ratio of the broad absorption line (BAL) QSOs [i.e. QSOs with blue absorption C IV and Ly $\alpha$  troughs of  $\Delta v/c \sim 0.04 - 0.1$  (e.g. Hewett & Foltz 2003; Srianand & Petitjean 2000)] is smaller than that of the QSO majority, possibly due to absorp-

---

<sup>1</sup> $\xi \equiv L/(nr^2)$  where  $L$  is an ionizing luminosity (between 1 and 1000 Ryd),  $n$  is the plasma number density and  $r$  is distance from the ionizing source.

tion of the X-rays by the BAL plasma. Indeed, this was confirmed by the *ASCA* detection of high X-ray absorption column  $N_H \geq 5 \times 10^{23} \text{ cm}^{-2}$  (Gallagher et al. 1999). Gallagher et al. (2006, hereafter, G06) later conducted a *Chandra* survey combined with known UV absorption properties that supported the earlier claims. The *Chandra* data of BAL QSOs indicate that  $\alpha_{\text{ox}}(\text{BAL}) \simeq -2.21$  (G06) is smaller than the mean QSO value  $\alpha_{\text{ox}}(\text{mean}) \simeq -2.0$ <sup>2</sup>. This result is augmented by a correlation between  $\alpha_{\text{ox}}$  and the 1 – 5 keV X-ray photon index  $\Gamma$ : increased photoelectric absorption of soft X-rays (i.e. smaller  $\alpha_{\text{ox}}$ ) also yields a smaller effective  $\Gamma$ , as observed.

The high outflow velocities of the prominent UV resonance lines (C IV and Ly $\alpha$ ) in BAL QSOs were traditionally ascribed to radiation-driven winds (Weymann et al. 1991), in analogy with the winds of O stars (Castor, Abbott & Klein 1975) and were modeled as such (e.g. Murray et al. 1995, hereafter, MCGV). MCGV recognized and included heuristically the effects of wind ionization and its shielding from the QSO X-rays, a crucial process as ionization reduces severely the effectiveness of line driving. Proga, Stone, & Kallman (2000, hereafter, PSK) presented 2D hydrodynamic simulations of these winds, including X-ray ionization, showing that the required shielding is provided by the section of the wind closest to the X-ray source that “failed” to launch by being too highly ionized, thereby allowing exterior segments to achieve velocities in agreement with C IV observations.

However, recent X-ray observations of BAL QSOs revealed absorption features in their spectra identified with highly ionized Fe XXV/Fe XXVI of column density  $N_H \sim 10^{23} - 10^{24} \text{ cm}^{-2}$ , blueshifted to high velocities  $v/c \sim 0.4 - 0.7$  (e.g. APM 08279+5255, PG 1115+080 and H 1413+117) indicating that X-ray ionization does not necessarily inhibit outflows, which can occur at velocities even higher than those seen in the UV lines (e.g., Chartas et al. 2002, 2003, 2007; Chartas et al. 2009, hereafter, C09). Additional X-ray studies have revealed a number of non-BAL QSOs that also exhibit similar X-ray absorbers at high velocities  $v/c \sim 0.1 - 0.5$  (e.g., Pounds et al. 2003 ; Reeves et al. 2003; Reeves et al. 2009), while in APM 08279+5255 C09 have also noted a correlation between  $\Gamma$  and the velocity of Fe XXV.

Motivated by these observations, we examine in this letter the conditions under which the magnetically-driven winds discussed in FKCB can reproduce the observed velocities of the BAL QSO X-ray features (Fe XXV) *along with* those of their more common UV transitions (C IV). In §2 we summarize the physics of MHD accretion disk winds and the differences of the ionization properties between Seyferts and BAL QSOs. In §3 we present our results and demonstrate a number of well-defined correlations among their kinematics, column, spectral index, and LoS angle and we conclude with a summary and discussion in §4.

---

<sup>2</sup>The spectral index  $\alpha_{\text{ox}} \equiv 0.384 \log(f_{2\text{keV}}/f_{2500})$  measures the X-ray-to-UV relative brightness where  $f_{2\text{keV}}$  and  $f_{2500}$  are respectively 2 keV and 2500 Å flux densities (Tananbaum et al. 1979)

## 2. The MHD Disk-Wind Model

In this section we present a brief outline of the MHD winds, originally formulated by Blandford & Payne (1982) and generalized by CL94 to include arbitrary distribution of axial current with radius. Here and in FKCB we focus on the current distribution that produces a density profile  $n(r) \propto r^{-1}$ , crucial for obtaining the observed AMD behavior. The same distribution leads also to a toroidal field  $B_\phi \propto r^{-1}$  that has equal magnetic energy per decade of (cylindrical) radius.

Self-similarity is assumed, i.e. power-law radial dependence for all variables and solution of the remaining angular part of these equations. As discussed in FKCB, this assumption is not very restrictive and justified *a posteriori* by the large number of decades of  $\xi$  in the AMD form.

The fundamental quantity of axisymmetric MHD is the magnetic stream function  $\Psi(r, \theta)$ , assumed to have the form  $\Psi(r, \theta) \equiv (r/r_o)^q \tilde{\Psi}(\theta) \Psi_o$ , with  $\Psi_o$  the poloidal magnetic flux through the fiducial wind launch radius at  $r = r_o$ .  $\tilde{\Psi}(\theta)$  is its angular dependence to be solved for and  $q \simeq 1$  a free parameter that determines the radial dependence of the poloidal current. The scalings of the poloidal magnetic stream function carry over to the rest of the wind properties of which we show only the magnetic field, velocity and density (see FKCB):

$$\mathbf{B}(r, \theta) \equiv (r/r_o)^{q-2} \tilde{\mathbf{B}}(\theta) B_o, \quad (1)$$

$$\mathbf{v}(r, \theta) \equiv (r/r_o)^{-1/2} \tilde{\mathbf{v}}(\theta) v_o, \quad (2)$$

$$n(r, \theta) \equiv (r/r_o)^{2q-3} \tilde{n}(\theta) B_o^2 v_o^{-2} m_p^{-1}, \quad (3)$$

where  $m_p$  is the proton mass. The dimensionless angular functions denoted by *tilde* must be obtained from the conservation equations and the solution of the Grad-Shafranov equation with initial values on the disk (denoted by the subscript “o”) at  $(r = r_o, \theta = 90^\circ)$ . The density normalization at  $(r_o, 90^\circ)$ , setting  $\tilde{n}(90^\circ) = 1$ , is given in terms of dimensionless mass-accretion rate  $\dot{m}$  (see FKCB) by

$$n_o = \frac{\eta_W \dot{m}}{2\sigma_T r_s}, \quad (4)$$

where  $\eta_W$  is the ratio of the mass-outflow rate in the wind to  $\dot{m}$ , assumed here to be of order unity and  $\sigma_T$  is the Thomson cross-section. It is important to note that because the mass flux in these winds depends in general on the radius,  $\dot{m}$  always refers to the mass flux at the innermost flow radius at  $r \simeq r_s$  where  $r_s$  is the Schwarzschild radius. In the present treatment we adopt the value  $q = 0.93$  resulting in  $n \propto r^{-1.14}$ , the steepest density dependence on  $r$  implied by the AGN AMD data of B09, and in order to allow for the somewhat higher observed X-ray column than UV column.

With the dimensionless, mass-invariant wind structure (see Fig. 1a) for given  $\dot{m}$  and  $\theta$ , the only significant difference in the wind ionization properties across objects of different

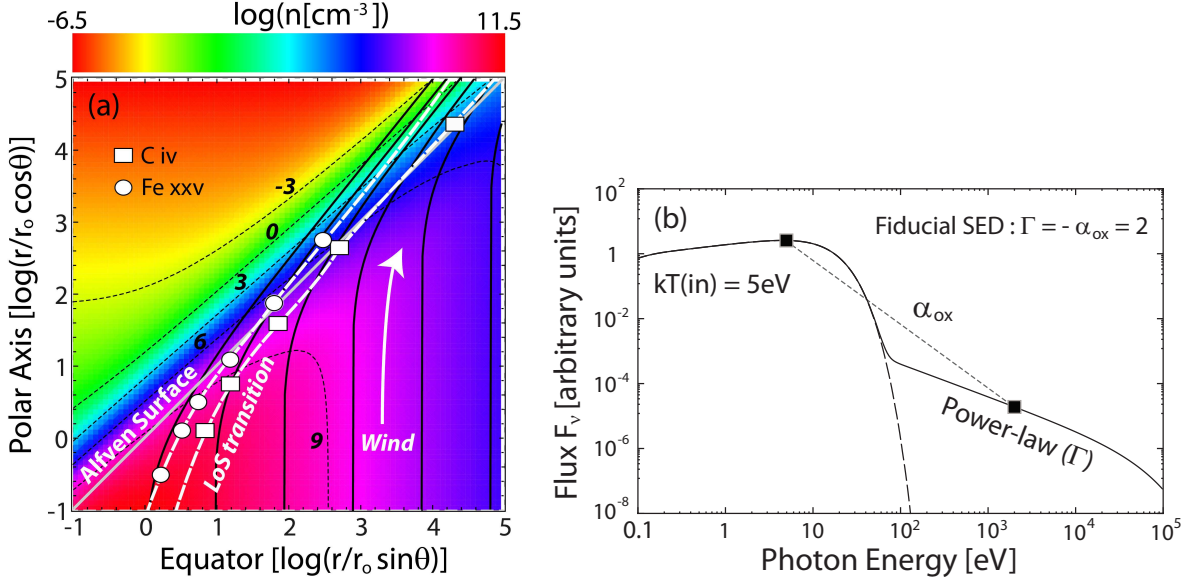


Fig. 1.— (a) Poloidal density structure  $\log(n[\text{cm}^{-3}])$  of MHD wind with  $\dot{m} = 0.5$ ; density contour curves (*dotted* lines with numbers) and magnetic field lines (*solid* curves) for  $M = 10^9 M_\odot$ . Also shown are the positions of the C IV (square =  $\square$ ) and Fe XXV (circle =  $\circ$ ) which shift outward along LoS of decreasing  $\theta$  [from  $80^\circ$  (innermost) to  $30^\circ$  (outermost) by a  $10^\circ$  increment]. Note that the C IV position for  $\theta = 30^\circ$  lies outside the figure range. (b) The form of the assumed input SED consisting of a thermal MCD of innermost temperature  $kT_{\text{in}} = 5 \text{ eV}$  and a PL continuum of photon index  $\Gamma$  normalized by  $\alpha_{\text{ox}}$ .

luminosity is the spectral distribution of ionizing radiation. While in FKCB we used a spectrum of the form  $F_\nu \propto \nu^{-1}$  (e.g. Sim et al. 2008, 2010), more appropriate for Seyferts, here we add a bright UV disk source. The spectrum used in the present work is shown in Figure 1b; it comprises a multicolor-disk (MCD) with an innermost temperature of 5 eV and an X-ray power-law (PL) of photon index  $\Gamma$  normalized by  $\alpha_{\text{ox}}$  (e.g. Everett 2005; Sim 2005). We do not include a soft X-ray excess in the SED, a feature more appropriate for narrow-line Seyfert spectra (e.g. Pounds et al. 2003; Sim 2005). The PL has a low energy cut-off at 5 eV and a high energy one at 200 keV. The total (X-ray plus UV) luminosity is  $L = 3 \times 10^{45} \text{ erg s}^{-1}$ .

### 3. Results

With the background flow ( $\dot{m} = 0.5$ ) and the spectrum of the ionizing radiation ( $\Gamma = -\alpha_{\text{ox}} = 2$ ) given, we follow the same procedure as in FKCB: we split the wind logarithm-

mically into a number of radial zones; we employ XSTAR to compute the ionization and opacities/emissivity in each zone along an observer’s LoS.

In Figure 2 we show the resulting distribution of the hydrogen-equivalent column densities  $\Delta N_H$  of iron and carbon for  $\theta = 50^\circ$  as a function of  $\xi$  (optimized here to model the outflows in APM 08279+5255) along with the corresponding LoS velocity (*dashed* curve), to be read on the right vertical axis. Note the well-defined velocity gradient of the wind with ionization parameter  $\xi$  due to its continuous structure. The Fe XXV ions identified through their resonance transitions of 1s-2p/3p obtain their peak hydrogen-equivalent columns of  $N_H(\text{Fe XXV}) \sim 2 \times 10^{23} \text{ cm}^{-2}$  at  $\log \xi \gtrsim 5$  with velocities  $v \gtrsim 0.5c$ . On the other hand, the C IV ions (2s-2p transitions) yield  $N_H(\text{C IV}) \sim 10^{23} \text{ cm}^{-2}$  with corresponding LoS velocities  $v \sim 0.1c$ , roughly consistent with the UV/X-ray absorbers in APM 08279+0255 data<sup>3</sup> (C09). The obtained ionization structure directly reflects the spatial positions of these ions; i.e.  $r(\text{Fe XXV})/r_s \sim 5 - 40$  and  $r(\text{C IV})/r_s \sim 200 - 700$  for  $\theta = 50^\circ$  (see Fig.1a) assuming a single LoS<sup>4</sup>. Note that the equivalent width (EW) of the modeled C IV absorption seems also to be fairly large due to a wide spread of its peak column distribution (i.e.  $1.5 \lesssim \log \xi \lesssim 4$ ) equivalent to  $\Delta v \sim 18,000 \text{ km s}^{-1}$  in agreement with the typical width of C IV BALs (i.e.  $\Delta v \sim 10,000 - 30,000 \text{ km s}^{-1}$ ).

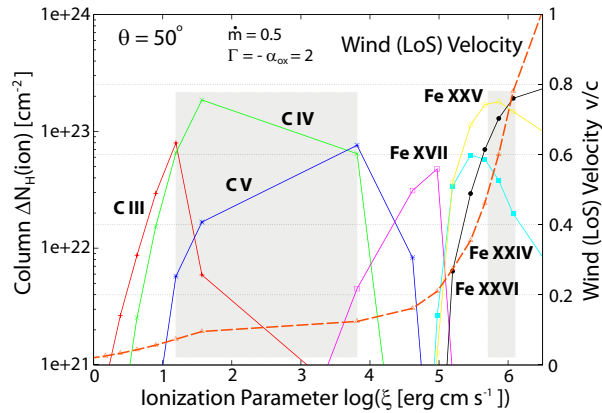


Fig. 2.— Simulated distribution of local column densities  $\Delta N_H$  (left ordinate) and the outflow velocity  $v$  (*dashed* curves; right ordinate) as a function of ionization parameter  $\xi$  for carbon and iron along the  $\theta = 50^\circ$  LoS. The shaded regions denote the parameter space (in  $\xi$  and  $v$ ) for which the local column is dominated primarily by C IV or Fe XXV.

<sup>3</sup>It is conceivable that scattered/reflected UV photons could externally fill in the “true” C IV absorption feature to seemingly reduce its intrinsic column (S. Kraemer, private communication).

<sup>4</sup>Different LoS for the UV/Optical and X-ray emitting regions (e.g. Dai et al. 2010) could alternatively be modeled with radiation transfer in a more complex source geometry.

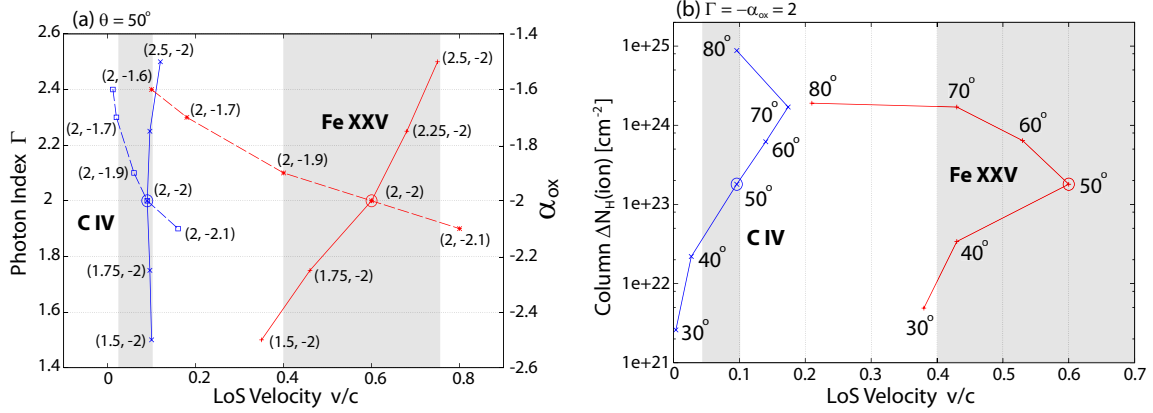


Fig. 3.— (a) Expected correlation of MHD wind velocity  $v$  with  $\Gamma$  (*solid* curves; left ordinate) and  $\alpha_{\text{ox}}$  (*dashed* curves; right ordinate) indicated by  $(\Gamma, \alpha_{\text{ox}})$  for C IV and Fe XXV with  $\dot{m} = 0.5$  and  $\theta = 50^\circ$ . (b) Expected correlation of wind velocity  $v$  with  $\Delta N_H$  and  $\theta$  (indicated by numbers in degree) for C IV and Fe XXV with  $\Gamma = -\alpha_{\text{ox}} = 2$ . Shared regions indicate the observed velocity dispersions of C IV and Fe XXV for APM 08279+5255.

The difference in the Fe XXV and C IV velocities above from those in FKCB [ $v(\text{Fe XXV}) \sim 3,000 \text{ km s}^{-1}$  and  $v(\text{C IV}) \sim 300 \text{ km s}^{-1}$ ] begs an explanation, considering the scale invariance of these winds and the similar values of  $\theta$  ( $\sim 50^\circ$ ) presented in both cases. This can be traced to the different  $\dot{m}$  and/or ionizing spectrum  $F_\nu$ . Indeed  $\dot{m}$  here is  $\sim 4$  times higher than that in FKCB, leading to a large increase in  $N_H$ ; furthermore,  $\alpha_{\text{ox}}$  is smaller here than in FKCB, with the present value  $\alpha_{\text{ox}} = -2$  consistent with the values of UV-luminous QSOs (Steffen et al. 2005).

These differences affect the Fe XXV and C IV velocities as follows: The combined increase in  $\dot{m}$  and decrease in  $\alpha_{\text{ox}}$  imply lower ionization of the plasma at the smallest  $r$ , despite the fact that the ratio  $L/n_o$  does not change; this is because the luminosity  $L$  in the definition of  $\xi$  involves an integral over the spectrum, while the ionization of the gas is affected mostly by the 2-10 keV X-rays. Therefore, an increase in  $\dot{m}$  for a given  $M$  achieves: (i) an increase in the plasma column, density and luminosity and (ii) a relative decrease of the ionizing hard X-ray flux (smaller  $\alpha_{\text{ox}}$ ). With these changes over FKCB, in the present treatment iron is not fully ionized even at the smallest radii ( $r \simeq 10r_s$ ), leading to  $v(\text{Fe XXV}) \simeq 0.7c$ . This partial ionization of the plasma, coupled with the increased column, reduces the ionizing flux that reaches further out into the wind, especially for high  $\theta$ , leading to a bootstrap of less ionization and increasingly higher soft X-ray opacity. Then, because of the ensuing severe reduction of ionizing photons in the  $E \sim 0.1 - 2 \text{ keV}$  range, the C IV ions form at smaller radii (higher velocities), so that the  $r^{-2}$  increase of the photon flux with  $E \gtrsim 64 \text{ eV}$  (the ionization potential of C IV) off-sets the photon depletion due to photoelectric absorption by

the partially ionized plasma.

Recent spectroscopic studies of BAL QSOs have indicated likely correlations between the maximum outflow velocity of the UV/X-ray absorbers and the spectral indices (G06;C09). For comparison we show in Figure 3a the modeled outflow velocities for C IV and Fe XXV with different values of  $(\Gamma, \alpha_{\text{ox}})$  for  $\dot{m} = 0.5$  and  $\theta = 50^\circ$ . It is seen for  $\alpha_{\text{ox}} = -2$  that Fe XXV velocities correlate strongly with  $\Gamma$  (*solid* curves) allowing for velocities in the range  $0.3 \lesssim v(\text{Fe XXV})/c \lesssim 0.8$  consistent with the X-ray outflow velocity observations in APM 08279+5255 (C09), while the C IV velocity is virtually unaffected. This is because for the steeper X-ray spectra fewer ionizing photons are available to produce highly-ionized species (e.g. Fe XXV of ionization potential  $\sim 9$  keV) and the relevant ions are found at smaller distances (higher velocities) than in the case of harder spectra. This does not affect significantly the overall ionization of the wind leaving the C IV transition at roughly the same distance. However, a change in  $\alpha_{\text{ox}}$ , affects strongly the maximum column position of both Fe XXV and C IV, as described above. For constant  $\Gamma (= 2)$ , the velocities of both these transitions correlate strongly with  $\alpha_{\text{ox}}$  (*dashed* curves), ranging between  $0.1 \lesssim v(\text{Fe XXV})/c \lesssim 0.8$  and  $0.01 \lesssim v(\text{C IV})/c \lesssim 0.15$  for  $-2.1 \lesssim \alpha_{\text{ox}} \lesssim -1.6$  qualitatively consistent with UV data (Laor & Brandt 2002; G06; Fan et al. 2009). Radiation forces are often invoked to explain these correlations (with X-ray shielding necessary for high velocities, e.g. MCGV;PSK). In contrast to these models, *high-velocity flows are always present in our model*, but only the steep  $\alpha_{\text{ox}} (\lesssim -2)$  allows the relevant ions (e.g., Fe XXV and C IV) to form in their *small-r, high-v regions* which are otherwise overionized (c.f. FKCB). While some (narrow-line) Seyferts with  $-1.6 \lesssim \alpha_{\text{ox}} \lesssim -1.1$  appear to exhibit X-ray outflows with  $v/c \lesssim 0.15$  (Dadina et al. 2005; Tombesi et al. 2010), these are systematically slower [and generally substantially slower (Holczer, Behar & Kaspi 2007; Holczer, Behar & Arav 2010)] than those of the BAL QSOs with  $\alpha_{\text{ox}} \lesssim -1.6$ . Thus, we propose  $\alpha_{\text{ox}}$  as the defining parameter that determines the velocities of the UV/X-ray absorption features in AGNs.

While the intrinsic MHD wind ionization structure is determined by  $\alpha_{\text{ox}}$ , the observables, i.e. the velocity widths/shifts of the ions depend strongly also on the observers' inclination angle  $\theta$ . In Figure 3b we present the LoS velocity of the C IV and Fe XXV transitions for various  $\theta$  with  $\Gamma = -\alpha_{\text{ox}} = 2$ . Because of the specific geometric shape of the magnetic field lines and ionization equilibria, characteristic ion velocities vary for different LoS angles [see also Fig. 1a for their positional transitions along various LoS from  $\theta = 80^\circ$  (innermost) to  $30^\circ$  (outermost)]. In this fiducial model we find that  $v_{\text{max}}(\text{Fe XXV}) \sim 0.6c$  at  $\theta \sim 50^\circ$  and  $v_{\text{max}}(\text{C IV}) \sim 0.15c$  at  $\theta \sim 70^\circ$ . At larger angles the velocities decrease but the integrated columns are so high that it is doubtful these features are observable. Similar diagrams can be computed for different values of the parameters  $(\dot{m}, \Gamma, \alpha_{\text{ox}})$  and can be directly compared to observations to assess the fundamental assumptions of these models.



#### 4. Summary & Discussion

We have demonstrated that purely MHD disk-winds with  $n \propto r^{-1}$ , originally proposed to account for the X-ray AMDs in Seyferts, can also encompass combined *high-velocity UV/X-ray absorber properties* as diverse as those of BAL QSOs, with those of APM 08279+5255 as a template. This is extremely important in view of the winds’ scale invariance, with the qualitative differences in the absorber properties between Seyferts and QSOs attributed mainly to their different  $\dot{m}$  and  $\alpha_{\text{ox}}$ . Given the well documented correlation of AGN UV-luminosity (a proxy for  $\dot{m}$ ) with  $\alpha_{\text{ox}}$  (Laor & Brandt 2002; Steffen et al. 2005; Fan et al. 2009), this model implies AGN absorber structure that depends essentially on a *single* parameter  $\alpha_{\text{ox}}$ . However, the observables, e.g., columns and velocities, depend additionally on the LoS angle  $\theta$ , reproducing the QSO BALs C IV (UV) and Fe XXV (X-ray) properties only for sufficiently large  $\theta$ , as usually considered.

Our calculations show that C IV forms at  $r/r_s \simeq 200 - 700$  with corresponding velocity  $v(\text{C IV}) \lesssim 0.1c$ . This value, along with the Fe XXV velocity  $v(\text{Fe XXV}) \simeq 0.6c$  at  $r/r_s \simeq 5 - 40$ , are consistent with those observed in APM 08279+5255 (C09). The shielding of the plasma from the X-rays at  $r \gtrsim 100r_s$ , necessary to produce the high velocity C IV absorption in radiation-driven wind models (MCGV;PSK), is in our case naturally provided by the *faster components of the same wind launched from even smaller radii*. Ionization equilibrium as a result of steeper  $\alpha_{\text{ox}}$  allows the relevant charge states to form closer to the central engines where the wind is faster.

For simplicity, we have ignored here a number of physical processes, e.g. radiation pressure (see PSK) and thermal instability (Krolik, McKee & Tarter 1981; Holczer, Behar & Kaspi 2007), likely to have an impact on our MHD-wind properties, that need to be implemented (e.g. Proga 2003). However, the broader validity of our models, gauged by the AMD dependence on  $\xi$ , will be decided by observations and quantitative analysis such as those presented in B09. It is also encouraging that the ionization properties of certain X-ray absorbers are consistent with this picture and, in fact, magnetic-driving of disk-winds has been favorably argued for GRO J1655-40 (e.g. Miller et al. 2008) and NGC 4151 (e.g. Crenshaw & Kraemer 2007), for example. We anticipate the upcoming *Astro-H* mission to contribute significantly to this goal by providing more detail on the Fe-K component of the wind, and thus to further clarify our picture of AGN structure.

Authors are grateful to the anonymous referee for inspirational suggestions. K.F. and D.K. would like to thank T. Kallman for insightful discussions, and G. Chartas, S. Kraemer, F. Tombesi and J. Turner for their constructive comments.

## REFERENCES

- Behar, E., 2009, ApJ, 703, 1346 (B09)
- Blandford, R. D & Payne, D. G. 1982, MNRAS, 199, 883
- Brandt, W. N., Laor, A., & Wills, B. J. 2000, ApJ, 528, 637
- Castor, J. I., Abbott, D. C. & Klein, R. I. 1975, ApJ, 195, 157
- Chartas, G., Brandt, W. N., Gallagher, S. C., & Garmire, G. P. 2002, ApJ, 579, 169
- Chartas, G., Brandt, W. N., Gallagher, S. C. 2003, ApJ, 595, 85
- Chartas, G., Eracleous, M., Dai, X., Agol, E., & Gallagher, S. C. 2007, ApJ, 661, 678
- Chartas, G., Saez, C., Brandt, W. N., Giustini, M., & Garmire, G. P. 2009, ApJ, 706, 644 (C09)
- Contopoulos, J., & Lovelace, R. V. E. 1994, ApJ, 429, 139 (CL94)
- Crenshaw, D. M. et al. 2003, Annu. Rev. Astro. Astrophys., 41, 117
- Crenshaw, D. M. & Kraemer, S. B. 2007, ApJ, 659, 250
- Dadina, M., Cappi, M., Malaguti, G., Ponti, G., & de Rosa, A. 2005, A&A, 442, 461
- Dai, X., Kochanek, C. S., Chartas, G., Kozłowski, S., Morgan, C. W., Garmire, G., & Agol, E. 2010, ApJ, 709, 278
- Everett, J. E. 2005, ApJ, 631, 689
- Fan, L. L., Wang, H. Y., Wang, T., Wang, J., Dong, X., Zhang, K., Cheng, F. 2009, ApJ, 690, 1006
- Fukumura, K., Kazanas, D., Contopoulos, I., & Behar, E. 2010, ApJ, 715, 636 (FKCB)
- Gallagher, S. C., Brandt, W. N., Sambruna, R. M., Mathur, S., & Yamasaki, N. 1999, ApJ, 519, 544
- Gallagher, S. C., et al. 2006, ApJ, 644, 709 (G06)
- Green, P. J., & Mathur, S. 1996, ApJ, 462, 637
- Holczer, T., Behar, E. & Arav, N. 2010, ApJ, 708, 981
- Holczer, T., Behar, E., & Kaspi, S. 2007, ApJ, 663, 799

- Hewett, P. C., & Foltz, C. B. 2003, *AJ*, 125, 1784
- Kallman, T., & Bautista, M. 2001, *ApJS*, 133, 221
- Krolik, J., McKee, C., & Tarter, 1981, *ApJ*, 249, 422
- Kopko, M., Turnshek, D. A., & Espey, B. R. 1994, in *IAU Symp. 159, Multiwavelength Continuum Emission of AGN*, ed. T. Courvoisier & A. Blecha (Dordrecht:Kluwer), 450
- Laor, A. & Brandt, W. N. 2002, *ApJ*, 569, L641
- Miller, J. M., Raymond, J., Reynolds, C. S., Fabian, A. C., Kallman, T. R., & Homan, J. 2008, *ApJ*, 680, 1359
- Murray, N., Chiang, J., Grossman, S. A. & Voit, G. M. 1995, *ApJ*, 451, 498 (MCGV)
- Pounds, K. A. et al. 2003, *MNRAS*, 345, 705
- Proga, D., Stone, J. M., & Kallman, T. R. 2000, *ApJ*, 543, 686
- Proga, D. 2003, *ApJ*, 585, 406
- Reeves, J. N., O'Brien, P. T., & Ward, M. J. 2003, *ApJ*, 593, L65
- Reeves, J. N. et al. 2009, *ApJ*, 701, 493
- Sim, S. A. 2005, *MNRAS*, 356, 531
- Sim, S. A., Long, K. S., Miller, L., & Turner, T. J. 2008, *MNRAS*, 388, 611
- Steffen, A. T. et al. 2005, *ApJ*, 131, 2826
- Sim, S. A., Miller, L., Long, K. S., Turner, T. J., & Reeves, J. N. 2010, 404, 1369
- Srianand, R. & Petitjean, P. 2000, *A&A*, 357, 414
- Tananbaum, H., et al. 1979, *ApJ*, 234, L9
- Tombesi, F. et al. 2010, accepted to *A&A*, arXiv:1006.2858
- Weymann, R. J., Morris, S. L., Foltz, C. B., & Hewett, P. C. 1991, *ApJ*, 373, 23